J Math Chem (2009) 46:781–794
DOI 10.1007/s10910-009-9544-2

ORIGINAL PAPER

Hydration effects on the reaction with an open-shell transition state: QM/MM-ER study for the dehydration reaction of alcohol in hot water

Hideaki Takahashi · Fumihiro Miki · Hajime Ohno · Ryohei Kishi · Suguru Ohta · Shin-ichi Furukawa · Masayoshi Nakano

Received: 16 December 2006 / Accepted: 30 September 2008 / Published online: 19 July 2009

Abstract The reaction mechanism for the dehydration of 1,4-butanediol in hot water has been investigated by means of the hybrid quantum mechanical/molecular mechanical approach combined with the theory of energy representation (QM/MM-ER). We have assumed that the proton transfers along the hydrogen bonds of the water molecules catalyze the reaction, where the transition state (TS) forms a singlet biradical electronic structure. It has been revealed by the simulation that the biradical electronic state at the TS changes to zwitterionic structure in solution due to the hydration of the polar solvent. Such the electronic structure change gives rise to the substantial stabilization of the TS in hot water. As a result, the water-catalytic path becomes more favorable in aqueous solution than another possible path that proceeds without proton transfers as opposed to the reaction mechanism in the gas phase. Furthermore, the activation free energy computed by the present method is in excellent agreement with the experimental result.

Keywords QM/MM · Real-space grids · Theory of energy representation · Free energy · Water solution

1 Introduction

The chemical event in a condensed phase is a matter of great interest since the electronic coupling between the chemically active site of the system and the remaining static environment is known to play a role in determining the reaction pathway [1]. In particular, it can be expected that the reaction mechanism of a solute with an open-shell electronic structure undergoes a serious change under the influence of the polar

H. Takahashi (✉) · F. Miki · H. Ohno · R. Kishi · S. Ohta · S. Furukawa · M. Nakano
Division of Chemical Engineering, Department of Materials Engineering Science, Graduate School of Engineering Science, Osaka University, Toyonaka, Osaka 560-8531, Japan
e-mail: takahasi@cheng.es.osaka-u.ac.jp

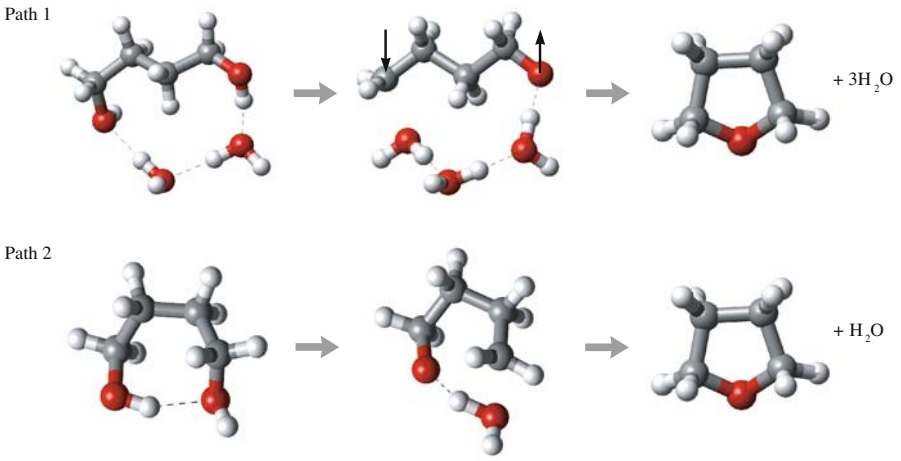

Fig. 1 Schematic representations of the two reaction paths assumed for dehydration of 1,4-butanediol. *Ball-and-stick* models are shown for reactants, transition states and products, respectively from *left* to *right*. *Up* and *down* electronic spins are drawn by *arrows* in the figure

solvent. Thus, the solvation effects on the reaction will become more important when the electronic wave function of the transition state (TS) forms a radical structure. The present paper addresses the issue of a chemical reaction in hot water that proceeds via a singlet biradical TS. Our interest will be focused on the electronic structure change of the TS due to the hydration for the purpose to determine the reaction pathway. A novel quantum mechanical method [2] combined with a theory of solution will be utilized to compute the free energy change associated with a chemical reaction in solution.

Nagai et al. [3] found that the dehydration of 1,4-butanediol, which leads to the tetrahydrofuran, takes place in hot water without any catalyst. Most importantly, their observation suggests that the solvent water molecules promote the reaction with its undissociated form eliminating the possibility that the solvent acts as an acidic catalyst. The previous quantum chemical studies [4] revealed that the ethanol oxidation reaction in the supercritical water is dramatically enhanced by the proton transfers along the hydrogen bonds of water wire. Based on these results, we make an assumption that the reaction proceeds through the proton transfers along the hydrogen bonds connecting the solute and solvent molecules. The reactant state has an electronically closed structure, however, the TS is in a singlet biradical state (path 1 in Fig. 1). Hence, the electronic coupling between the solute and solvent is expected to be so significant as to influence the reaction mechanism. To make comparisons, we also consider another possible reaction path where dehydration process takes place directly without proton transfers (path 2 in Fig. 1). The difference in the hydration effects between the two reaction paths will be discussed.

Free energy change associated with a chemical reaction, of course, plays an essential role in determining the reaction pathway. The quantum chemical approach [5] based on the first principles is essential for the study of chemical reactions, however, it generally requires much computational cost even at the low levels of theory. In addition, a substantial amount of ensemble for molecular configurations is needed to attain the convergence of the free energy when the system consists of many particles [6,7].

Therefore, it is a heavily demanding task to compute the free energy for a reaction in a condensed system. In this paper, we present a novel approach to the free energy calculation by utilizing the hybrid quantum mechanical/molecular mechanical method [8,9] combined with the theory of energy representation (QM/MM-ER) [2] recently developed by Takahashi and Matubayasi. Within the theory of energy representation proposed by Matubayasi and Nakahara [10–12] the distribution of the solute–solvent interaction plays a fundamental role in determining the excess chemical potential of the solute. This is differed from the conventional theory of solution [13] where the free energy is expressed in terms of the spatial distribution functions of the solvent around the solute. It is worthy of note that a set of interaction sites, which is an artificially simplified model of a real molecule, is no longer needed to construct the distribution functions within the framework of the theory of energy representation. The internal degrees of freedom of the solute molecule can also be naturally incorporated into the free energy calculations. By virtue of these advantages, one can straightforwardly take into consideration the spatially diffuse nature of the electron density and its fluctuation, which are inherent in the quantum mechanical object, through the QM/MM-ER approach. Furthermore, the computational cost required to calculated the free energy change by the QM/MM-ER is much smaller as compared with the numerically exact method such as free energy perturbation or thermodynamic integration and its application for a larger system can be accomplished under the modest computational environment.

We apply the QM/MM-ER method to compute the free energy change associated with the dehydration reaction of alcohol assisted by the proton translocation along the water wire. The solvation free energies for the reactant and TS are decomposed into several contributions, such as electron density polarization or fluctuation. In the following, we review an outline of the methodology and describe the computational details. The results and discussion is presented in the subsequent section.

2 Methodology

The notable features of our methodology (QM/MM-ER) are summarized in two points. One is that the real-space grid approach [14–17] is employed to express the one-electron wave functions in Kohn–Sham density functional theory (DFT) [18,19] and the other is that the solvation free energy of a solute is described in terms of the distribution functions of the solute–solvent interaction energy. The following subsections are devoted to the review of these method as well as the description for the computational details.

2.1 The real-space grid approach

Within the framework of the Kohn–Sham DFT, the equation for the QM/MM simulation can be described as [15],

$$\left(-\frac{1}{2}\nabla^2 + \int \frac{n(\mathbf{r}')}{|\mathbf{r}-\mathbf{r}'|}\mathrm{d}\mathbf{r}' + v_{\mathrm{ps}} + \frac{\delta E_{\mathrm{xc}}(n(\mathbf{r}))}{\delta n(\mathbf{r})} + V_{\mathrm{pc}}(\mathbf{r})\right)\varphi_i(\mathbf{r}) = \varepsilon_i\varphi_i(\mathbf{r}) \quad (1)$$

where $n(\mathbf{r})$ is the electron density, v_{ps} represents the pseudopotentials of atoms, E_{xc} is the exchange correlation functional, and finally V_{pc} expresses the electrostatic field formed by the point charges on the solvent molecules described by molecular mechanics. The one-electron wave functions are expressed by the values on the real-space grids uniformly distributed over a cubic QM cell. Accordingly, the Laplacian in Eq. 1 is approximated by a finite-difference scheme as proposed by Chelikowsky et al. [16] thus,

$$
\begin{aligned}
-\frac{1}{2}\nabla^2\varphi_i(x_i, y_j, z_k) = -\frac{1}{2h^2}\Bigg[& \sum_{n=-N}^{N} C_n\varphi_i(x_i + nh, y_j, z_k) \\
& + \sum_{n=-N}^{N} C_n\varphi_i(x_i, y_j + nh, z_k) \\
& + \sum_{n=-N}^{N} C_n\varphi_i(x_i, y_j, z_k + nh)\Bigg],
\end{aligned} \tag{2}
$$

where (x_i, y_j, z_k) is the coordinate of the grid, h is the grid-spacing, and C_n are the expansion coefficients. Recently, Takahashi et al. [20–24] developed a novel code for the QM/MM simulations by utilizing the real-space grids and confirmed the accuracy and the efficiency of the method. The advantage of the approach in the DFT is that it is straightforward to compute the exchange-correlation energy E_{xc} of the system. Actually, even in the LCAO approach [5], the integration for the E_{xc} energy is performed over the real-space grids that are radially distributed around the nuclei. By virtue of the locality of the Exc operator in DFT, most of the operators in Eq. 1 becomes local and the hamiltonian matrix elements in the real-space representation are confined within a small region of space. Therefore, the parallel implementation in the real-space approach is amenable and the high performance computing can be realized. Actually, in the previous calculations on a larger system, we demonstrated the high efficiency of the present approach [25].

2.2 Theory of energy representation

Within the conventional theory of solution, the solvation free energy of a solute of interest is described in terms of the spatial distribution functions of solvent around the solute [10]. In practice, the set of site-site radial distribution functions, which is a reduced form of the full coordinate description, is commonly used due to the computational and conceptual convenience. In the method of energy representation, on the other hand, the statistical molecular configuration is represented by the distribution function of the solute–solvent interaction energy. We give the definition of the energy distribution function $\rho(\varepsilon)$ below.

Let $v(\mathbf{x})$ be the solute–solvent interaction potential of interest, where $\mathbf{x}$ is the full coordinate (position and orientation) of the solvent molecule relative to the solute fixed at the origin with a fixed orientation. The instantaneous distribution in the energy representation can be written as

$$\hat{\rho}(\varepsilon) = \sum_i \delta(v(\mathbf{x}_i) - \varepsilon) \tag{3}$$

where $\mathbf{x}_i$ is the full coordinate of the ith solvent molecule, $v(\mathbf{x})$ is the two-body interaction energy between the solute and solvent and the sum is taken over solvent molecules. Here, we define the energy distribution $\rho(\varepsilon)$ as the ensemble average of Eq. 3 in the solution and the distribution $\rho_0(\varepsilon)$ as the ensemble average for the pure (reference) solvent system where the solute molecule is placed in the neat solvent as a test particle. Then, the solvation free energy $\Delta\bar{\mu}$ of the solute can be expressed exactly as

$$\Delta\bar{\mu} = -k_B T \int d\varepsilon \left[(\rho(\varepsilon) - \rho_0(\varepsilon)) + \beta\omega(\varepsilon)\rho(\varepsilon) - \beta \left(\int_0^1 d\lambda \omega(\varepsilon; \lambda) \right) (\rho(\varepsilon) - \rho_0(\varepsilon)) \right] \tag{4}$$

where $\omega(\varepsilon)$ is the indirect part of the solute-solvent potential of mean force and β is the inverse of the Boltzmann constant k_B multiplied by the temperature T. λ in Eq. 4 is the coupling parameter associated with the gradual insertion of the solute in the solvent. In the practical implementation, integration with respect to λ is performed approximately by adopting a hybrid functional of PY and HNC [11].

In the development of Eq. 3, it is assumed that the solute–solvent interaction is pairwise additive. However, the electron density of the QM solute is determined under the interaction with a number of solvent molecules. The solute–solvent interaction then involves many-body effects and is not pairwise. We consider the QM solute with the electron density $\tilde{n}(\mathbf{r})$ fixed at its average distribution in solution. Then, the total solvation free energy $\Delta\mu$ of the QM solute can be decomposed as [2]

$$\Delta\mu = \Delta\bar{\mu} + \bar{E} + \delta\mu \tag{5}$$

where $\Delta\mu$ is the solvation free energy of the solute with the density $\tilde{n}(\mathbf{r})$, $\bar{E}$ is the average distortion energy of the QM solute, and the remaining term $\delta\mu$ represents the contribution due to the many-body effect. The distortion energy $\bar{E}$ of the solute can be defined by

$$\begin{aligned} \bar{E} &= \langle \langle \Psi_{sol} | \mathbf{H}_0 | \Psi_{sol} \rangle - E_0 \rangle \\ &= \frac{\int d\mathbf{X} (\langle \Psi_{sol} | \mathbf{H}_0 | \Psi_{sol} \rangle - E_0) \exp(-\beta(E_{QM} + E_{QM/MM} + E_{MM}))}{\int d\mathbf{X} \exp(-\beta(E_{QM} + E_{QM/MM} + E_{MM}))} \end{aligned} \tag{6}$$

where $(E_{QM} + E_{QM/MM} + E_{MM})$ expresses the total energy of the QM/MM system, and $\mathbf{X}$ the configuration of the solvent molecules collectively. Ψ_{sol} in Eq. 6 denotes the instantaneous total wave function of the QM solute in solution, and $\mathbf{H}_0$ and E_0 represent the hamiltonian and the energy of the solute at isolation, respectively. $\Delta\mu$ is the free energy originating from the two-body part in the QM/MM potential and can be computed directly from Eq. 4. The free energy $\delta\mu$ in Eq. 5 can be estimated separately

by introducing another energy coordinate corresponding to the electron density deviation from $\tilde{n}(\mathbf{r})$ [2,12]. The major contribution to the total free energy can be given, of course, by the leading two terms in r.h.s of Eq. 5 in ordinary cases. The efficiency and accuracy of the QM/MM combined with the theory of energy representation were well examined by previous works [2,26,27].

2.3 Computational details

The free energy difference δG_{aq} between the TS and the reactant in the aqueous solution can be expressed as

$$\begin{aligned}\delta G_{\mathrm{aq}} &= G_{\mathrm{vibrot}}(\mathrm{TS}) + E_{\mathrm{ZPE}}(\mathrm{TS}) + \Delta\mu(\mathrm{TS}) + E_{\mathrm{gas}}(\mathrm{TS}) \\ &\quad -\{G_{\mathrm{vibrot}}(\mathrm{R}) + E_{\mathrm{ZPE}}(\mathrm{R}) + \Delta\mu(\mathrm{R}) + E_{\mathrm{gas}}(\mathrm{R})\} \\ &= \Delta\mu(\mathrm{TS}) - \Delta\mu(\mathrm{R}) + \delta G_{\mathrm{vibrot}} + \delta E_{\mathrm{ZPE}} + \delta E_{\mathrm{gas}}, \end{aligned} \tag{7}$$

where $G_{\mathrm{vibrot}}(\mathrm{TS})$ and $G_{\mathrm{vibrot}}(\mathrm{R})$ denote the free energies associated with the vibration and rotation for the TS and the reactant, respectively and $\Delta\mu$ represents the solvation free energies of the solutes. The notation δ corresponds to the change from the reactant to the TS. E_{ZPE} in Eq. 7 denotes the correction by the zero-point vibrational energy.

We have optimized the molecular geometries for the reactant and the TS by means of the KS-DFT with B3LYP functional [28,29] and 6-31G* basis set. The geometry optimizations for the TS have been performed by the Synchronous Transit-guided Quasi-Newton (STQN) algorithm [30] in Gaussian 98 [31]. Since the TS of the path 1 has the singlet biradical electronic structure, spin-unrestricted Kohn–Sham wave functions have been used to construct the electron density. Since the electronic state of the TS of path 1 undergoes the serious solvation effects of the polar solvent, the structure of the TS will be substantially deformed due to the hydration. We have tried to optimize the TS structure with the PCM approach to mimic the exsistence of the solvent, however, the zwitterionic electronic structure have not been realized under the solvent of uniform dielectric constant. Thus, the energy change in the TS due to the structure change by the solvation could not be estimated. In the QM/MM simulation, the QM solute has been described by KS-DFT with BLYP functional [32], where the QM cell has been discretized by 64 grids in one dimension. The nonlocal pseudopotential in the Kleinman–Bylander form [33] has been used for the term v_{ps} in Eq. 1. The OPLS all-atom model [34] has been adopted for the Lennard–Jones parameters for the QM solute. The MM water solvent has been represented by 252 TIP4P water molecules [35]. The thermodynamic condition has been set at $T = 575\,\mathrm{K}$ [36] and $\rho = 0.6\,\mathrm{g/cm^3}$. The NVT ensembles have been generated through the leap-frog algorithm [6], where the time step has been set at 1.0 fs. The experiments were carried out under the higher temperatures (658, 673 K), however, the simulations at the lower temperature have been intended to see the solvation effect clearly. The QM/MM simulations have been carried out for 50 ps to obtain average electron density $\tilde{n}(\mathbf{r})$, followed by 100 and 200 ps simulations to construct the energy distribution functions $\rho(\varepsilon)$ and $\rho_0(\varepsilon)$, respectively. In this procedure, we have only considered the solvent molecules inside a sphere of which center is taken as the center of mass of the solute.

In the present simulation radius of the sphere has been set at nine. In order to investigate the polarization effects of the electron density of the QM solute in polar solvent, we have also computed the solvation free energies of the solutes with electron densities at isolation.

3 Results and discussion

Figures 2 and 3 show the optimized molecular geometries of the reactants and the TSs for path 1 and 2, respectively.

In the Fig. 2, two water molecules make a hydrogen-bonded complex with 1, 4-butanediol at the reactant of path 1, which leads to the TS through the concerted

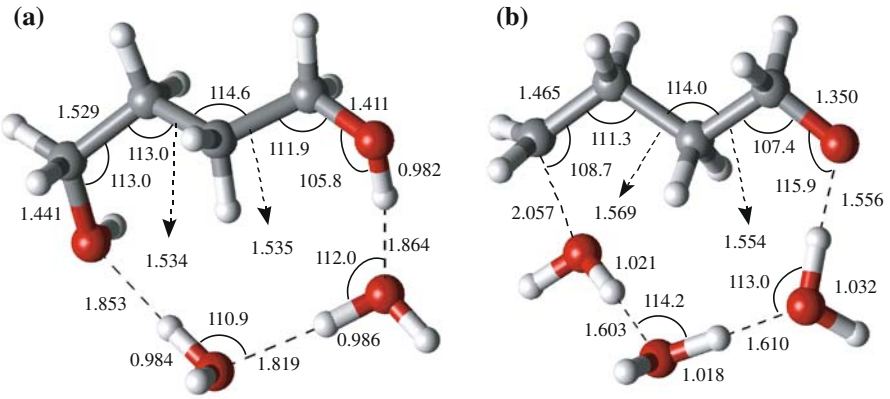

Fig. 2 Optimized geometries of **a** the reactant and **b** the TS for path 1. The angles and bond distances are in the units of degree and angstroms, respectively

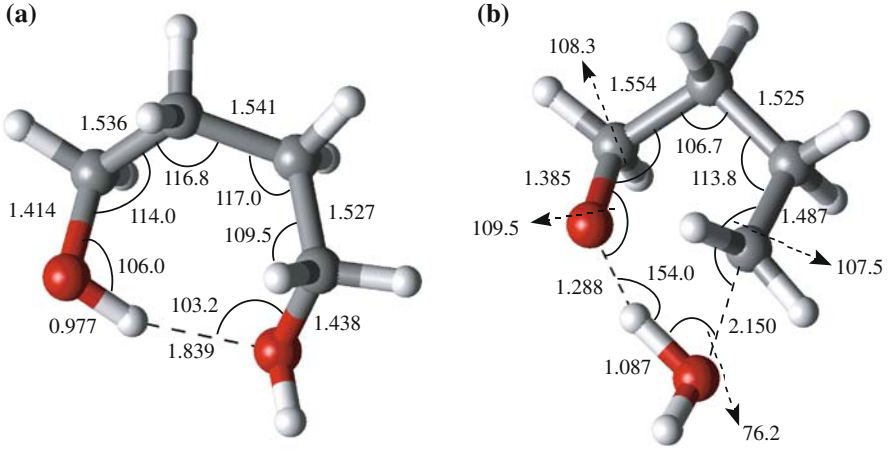

Fig. 3 Optimized geometries of **a** the reactant and **b** the TS for path 2. The angles and bond distances are in the units of degree and angstroms, respectively

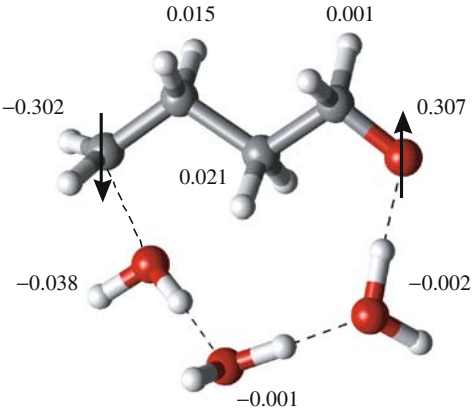

Fig. 4 Mulliken spin populations on heavy atoms of the TS of path 1, where the values on hydrogen atoms are summed into nearest heavy atoms

proton transfers along the hydrogen bonds. It can be recognized that the three water molecules are almost formed at the TS of path 1. After this process, three water molecules and an unstable biradical intermediate are generated. The reaction is completed by the subsequent cyclization of the intermediate. At the reactant of path 2 (Fig. 3), an intramolecular hydrogen bond is formed. As opposed to path 1, the direct dehydration and the cyclization take place simultaneously in path 2 as expected from the molecular structure of the TS. Although the geometry optimizations have been done by the B3LYP/6-31G* level, we have computed the energy change δE_{gas} in Eq. 7 by using the BLYP functional with the aug-cc-pVDZ basis set [37] because only the BLYP can be utilized as a generalized gradient approximations (GGA) functional in our QM/MM code based on the real-space grid approach. The sum of last three terms in Eq. 7 has been computed as 62.0 and 53.0 kcal/mol for path 1 and 2, respectively. Thus, in the gaseous phase, path 2 is obviously much more favorable as compared with path 1.

Since path 1 proceeds via the biradical intermediate, it is possible that the TS also has biradical electronic structure. We have computed Mulliken spin population on each heavy atom for the TS with the symmetry-broken wave function. For the clarity and simplicity, the population on hydrogen atoms are summed into nearest heavy atoms. The computational method is the unrestricted Kohn–Sham DFT employing the B3LYP functional and the 6-31G* basis set. The result is shown in Fig. 4.

It has been found that large spin density localizes on the oxygen of the 1,4-butanediol and the opposite spin on the CH_2-group, which are associated with the O–H and C–O bond dissociations, respectively. On the other hand, spin densities on the water molecules or CH_2-groups with sp_3-carbon are relatively small. Thus, it has been revealed that the TS of path 1 has clearly biradical character. Note that the spin population will become more remarkable when we employ the unrestricted Hartree–Fock method [5] since the exchange functional based on the local density approximation in DFT itself simulates the static correlation to a certain extent. On the contrary to path 1, the spin-population on each atom for path 2 has been computed to be zero indicating that the TS has closed electronic structure. Thus, the electronic structures for the two reaction paths are quite different in nature and it will make a substantial difference in the solvation effects.

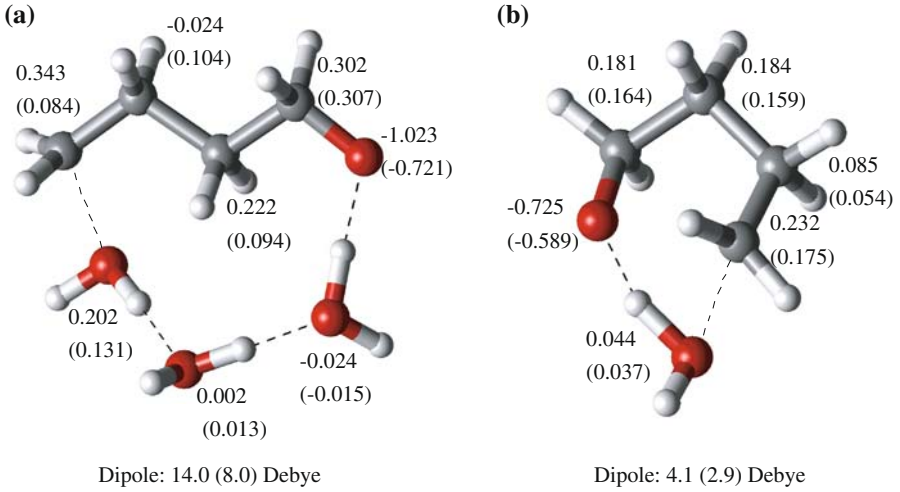

Fig. 5 Optimized fractional charges on heavy atoms of the TSs of **a** path 1 and **b** path 2 in units of elementary charge, where the values on hydrogen atoms are summed into nearest heavy atoms. The values in the *parentheses* are those obtained in the gas phase

As described in the section of Methodology, we have performed a 50-ps QM/MM simulation in solution to obtain the average electron distributions $\tilde{n}(\mathbf{r})$ of a QM solute. Subsequently, 100 and 200-ps simulations have been carried out for the solute with $\tilde{n}(\mathbf{r})$ to construct the energy distribution functions for the solution and the reference systems, respectively. The fractional charge allotted to each atom of the solute with the electron density $\tilde{n}(\mathbf{r})$ gives useful information such as the degree of electron density polarization due to hydration. The charge optimization has been done by least-square fittings to reproduce the realistic electrostatic potential formed by $\tilde{n}(\mathbf{r})$ and the nuclei. The details of the method are given in Ref. [38]. The fractional charges for the TSs of path 1 and 2 are presented in Fig. 5.

In the TS of path 1, a large negative charge localizes on the oxygen of the 1,4-butanediol and a positive charge on the CH_2-group at the end of the molecule. The population changes due to the solvation at these sites are very large (O: -0.30 e, CH2: $+0.26$ e). It should be noted that the electronic polarization is significant at the sites where the spin has large populations at isolation. Since the two fractional charges with opposite signs locate with a long distance, the TS has a large dipole moment (14.0 Debye) which is much larger than that of the gas phase (8.0 Debye). Such the difference in the dipole is of course due to the density polarization of the TS in solution. As for the TS of path 2, fractional charge has the largest absolute value of -0.725 at the oxygen and the positive charge is distributed over the CH_2-groups and the leaving water molecule. Thus, the density polarization of path 2 is much smaller than that of path 1 and it is confined within a small region of space. Hence, the electrostatic interaction of the TS of path 2 with the aqueous environment is expected to be rather weak as compared with path 1.

The energy distribution functions have been constructed to compute solvation free energies of the solute molecules with average electron density $\tilde{n}(\mathbf{r})$. As a special

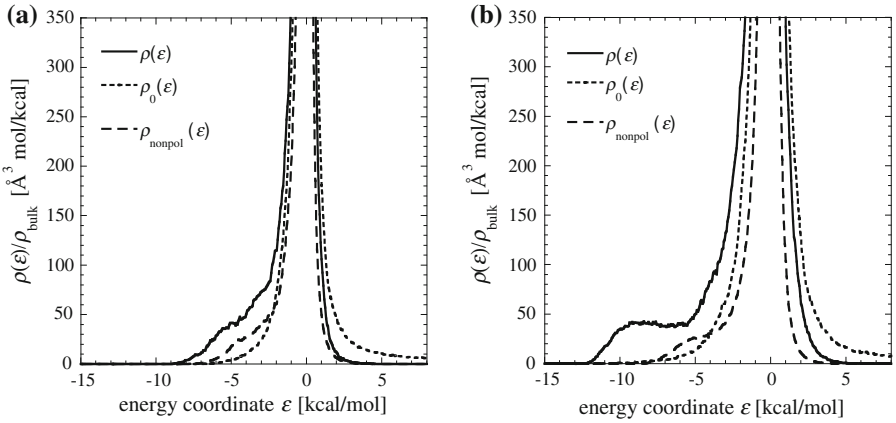

Fig. 6 Energy distribution functions for **a** the reactant and **b** the TS of path 1. $\rho(\varepsilon)$ is for the solution, and $\rho_0(\varepsilon)$ for the pure solvent system. $\rho_{\text{nonpol}}(\varepsilon)$ is the distribution function for the QM solute with non-polarized electron density. The distributions are normalized by the bulk number density ρ_{bulk}

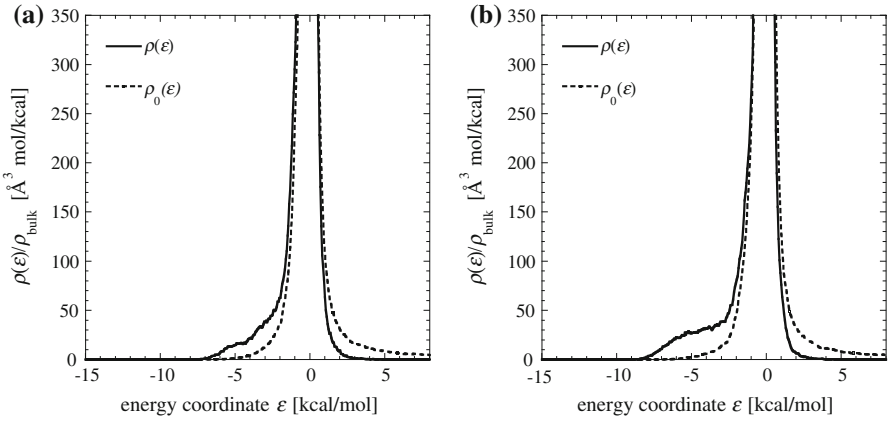

Fig. 7 Energy distribution functions for **a** the reactant and **b** the TS of path 2. $\rho(\varepsilon)$ is for the solution, and $\rho_0(\varepsilon)$ for the pure solvent system. The distributions are normalized by the bulk number density ρ_{bulk}

treatment for path 1, we have also computed the solvation free energies of the solutes with electron density at isolation to study the contribution of the density polarization. The energy distribution functions for path 1 and 2 are presented in Figs. 6 and 7, respectively.

In the distribution function for the TS of path 1 (Fig. 6b) a distinct peak appears around −10 kcal/mol on the energy coordinate, which differs from that for the reactant (Fig. 6a). Since the distribution on the lower energy coordinate indicates that the solute–solvent interaction is more favorable, it is expected that the TS is much stabilized in the hot water as compared with the reactant. It should also be noted that the energy distribution of the non-polarized TS has only a slight peak around −5 kcal/mol on the energy coordinate in contrast to the solute with $\tilde{n}(\mathbf{r})$. The effect of the polarization on the reactant of path 1 has been found to be modest. The fact that the polarization effect

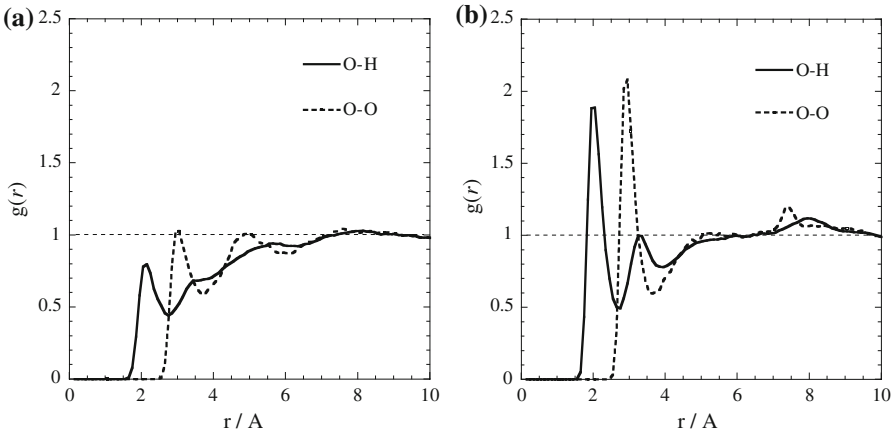

Fig. 8 Radial distribution functions for **a** the reactant and **b** the TS. The *real* and the *broken lines* are, respectively, for the hydrogen and oxygen atoms of solvent water molecule around the oxygen that undergoes the OH bond dissociation in 1,4-butanediol

Table 1 The solvation free energies and their components in unit of kcal/mol

	$\Delta\mu_{\rm sol}$					$\Delta\mu_{\rm sol}$
	$\bar{E}$	$\Delta\bar{\mu}_{\rm pol}$	$\Delta\bar{\mu}_{\rm nonpol}$	$\delta\mu$	$\Delta\mu_{\rm onsager}$	
Reactant	4.1	−3.3	−3.4	−3.9	−0.2	−6.7
TS	15.5	−18.3	−8.8	−5.6	−1.8	−19.0

The thermodynamic condition is $\rho = 0.6\,{\rm g/cm^3}$ and $T = 575\,{\rm K}$. $\Delta\mu$ in Eq. 5 is further decomposed into the contributions due to the electron density polarization $\Delta\bar{\mu}_{\rm pol}$ and the non-polarized solute $\Delta\bar{\mu}_{\rm nonpol}$

on the TS of path 1 is significant is consistent with the result of the fractional charge analyses shown in Fig. 5. One can see in Fig. 7 no remarkable change in the energy distribution functions between the reactant and the TS of path 2 except the slight increase in the distribution of the TS on the energy coordinate around −5 kcal/mol.

Next, we show the radial distribution functions of the solvent water molecules around the oxygen atom that has a large spin population at the TS in path 1 (see Fig. 4). The comparisons have been made between the reactant and the TS (Fig. 8).

One can see that a drastic change takes place in the solvation structure when the solute goes from the reactant to the TS. The two peaks corresponding to the hydrogen bonds largely increase their intensity at the TS, which can be attributed to the electronic polarization of the TS. These simulations so far implies that path 1, differed from path 2, will undergo a serious solvation effect due to the stabilization of the TS by the hot water.

We finally present the results of the solvation free energies obtained by the QM/MM simulations combined with the theory of energy representation to discuss in detail the solvation effect and also the mechanism of the dehydration reaction in the hot water. Table 1 shows the solvation free energies and their components for the reactant and the TS of path 1. The average distortion energy $\bar{E}$ of the QM solute defined by Eq. 6

expresses the degree of the density polarization. $\bar{E}$ of the TS has been computed as 15.5 kcal/mol that is nearly 4-times as large as that of the reactant. Distortion of the wave function, of course, destabilizes the QM solute in the solution, however, it also makes a substantial contribution to the stabilization through the electrostatic interaction with the polar solvent. Actually, the solvation free energy $\Delta\bar{\mu}_{\rm pol}$ of the polarized solute has been estimated as −18.3 kcal/mol at the TS. Thus, we have estimated the net gain due to the density polarization as −2.8 kcal/mol for the TS. The solvation free energy $\Delta\bar{\mu}_{\rm nonpol}$ of the non-polarized solute has been found to give dominant contribution (−8.8 kcal/mol) to the total solvation free energy of the TS. The free energies $\delta\mu$ associated with the electron density fluctuations have also been computed by doing additional QM/MM simulations. The free energy for the TS is −5.6 kcal/mol and the reactant has also non-negligible value of −3.9 kcal/mol. It has been revealed that the contribution of $\delta\mu$ to the total solvation free energy cannot be overlooked, though its difference between the reactant and the TS is not so large. As noted in Methodology, the energy distribution functions have been constructed for the solvent molecules inside a sphere containing the solute. In the present simulation, radius of the sphere has been set at nine. The Onsager correction $\Delta\mu_{\rm onsager}$ represents the contribution from the infinite bulk continuum outside the sphere. $\Delta\mu_{\rm onsager}$ has been estimated in unit of kcal/mol by the following equation [39], thus,

$$\Delta\mu_{\rm onsager} = 7.19652\frac{2\varepsilon - 2}{2\varepsilon + 1}\frac{d^2}{r^3}, \tag{8}$$

where dielectric constant ε is set at 15.3 and d is the dipole moment of the solute in Debye and r is the radius of the sphere in. The large dipole moment of the TS gives rise to the significant contribution (−1.8 kcal/mol) from the bulk solvent outside the sphere. The sum of these terms gives total solvation free energy $\Delta\mu$. It has been found that the solvation free energy $\Delta\mu$ of the TS (−19.0 kcal/mol) is much larger than that of the reactant (−6.7 kcal/mol). Substituting these values into Eq. 7, the free energy change $\delta G_{\rm aq}$ in aqueous solution can be obtained as 49.7 kcal/mol for path 1. As for path 2, the solvation free energies $\Delta\mu$ for the reactant and TS have been computed as 0.0 and −0.9 kcal/mol, respectively, from which we get the activation free energy for path 2 as 52.1 kcal/mol. Note that the free energy $\delta\mu$ due to the electron density fluctuation has not been computed for path 2 since the difference in $\delta\mu$ can be considered to be negligible because of the weak solute–solvent interaction. The activation free energy obtained by the experimental observation was reported as 50 kcal/mol in accord with the present results. The QM/MM-ER simulations have revealed that path 1 is more favorable than path 2 in the hot water on the contrary to the reaction in the gas phase. Another aspect that affects the reaction pathway is the probabilities of the reactant states for path 1 and 2. It has been shown that the reactant of path 1 is more stable than that of path 2 by 11.7 kcal/mol with the calculations of B3LYP/6-31G* levels. Although the solvation free energies for the reactants must be also taken into considerations, it seems that the reactant of path 1 is more preferable in hot water. The mechanism responsible for the dramatic change of the reaction path due to the hydration can be explained by a qualitative discussion that the biradical electronic state of the TS of path 1 changes to a zwitterionic structure in the polar solvent to gain

the electrostatic stabilization energy. Such the picture can be naturally deduced from the results of the analyses of spin density, fractional charges, and radial distribution functions given in the previous figures.

4 Conclusions

In the present study, we carried out the QM/MM simulations combined with the theory of energy representation (QM/MM-ER) to compute the free energy change associated with the dehydration reaction of 1,4-butanediol in aqueous solution. Two possible reaction paths were examined to study the reaction mechanism in the hot water. In path 1, we assume that two water molecules make a hydrogen-bonded complex with 1,4-butanediol and then concerted proton transfers along the water wire lead to a TS based on the results of the ethanol oxidation reaction in the supercritical water. On the other hand, in path 2, dehydration takes place directly without no participation of water molecules in the reaction. The QM/MM simulations showed that the biradical TS forms a zwitterion in polar solvent giving rise to significant stabilization contrary to the TS of path 2. As a result, path 1 becomes slightly favorable as compared with path 2 in the aqueous solution, though path 2 is obviously the major channel in the gas phase. Thus, it was demonstrated by the state-of-the-art method that the water molecule catalyzes the dehydration of 1,4-butanediol in the hot water in its undissociated form in agreement with the suggestion given by the experiment.

Acknowledgments The present study is supported by Grants-in-Aid for Scientific Research (No. 15360422), and the NAREGI (National Research Grid Initiative) Project from the Ministry of Education, Culture, Sports, Science and Technology in Japan.

References

1. P.J. Rossky, J.D. Simon, Nature **370**, 263 (1994)
2. H. Takahashi, N. Matubayasi, T. Nitta, M. Nakahara, J. Chem. Phys. **121**, 3989 (2004)
3. Y. Nagai, N. Matubayasi, M. Nakahara, Bull. Chem. Soc. Jpn. **77**, 691 (2004)
4. H. Takahashi, S. Hisaoka, T. Nitta, Chem. Phys. Lett. **363**, 80 (2002)
5. A. Szabo, N.S. Ostlund, *Modern Quantum Chemistry* (Macmillan, New York, 1982)
6. M.P. Allen, D.J. Tildesley, *Computer Simulation of Liquids* (Oxford University Press, Oxford, 1987)
7. D. Frenkel, B. Smit, *Understanding Molecular Simulation from Algorithms to Applications, Computational Science Series,* vol 1 (Academic Press, New York, 2002)
8. J. Gao, M.A. Thompson (eds.), *Combined Quantum Mechanical and Molecular Mechanical Methods* (American Chemical Society, Washington, DC, 1998)
9. M.F. Ruiz-Lopez (ed.), Combined QM/MM calculations in chemistry and biochemistry. J. Mol. Struct. (THEOCHEM) **632** (2003)
10. N. Matubayasi, M. Nakahara, J. Chem. Phys. **113**, 6070 (2000)
11. N. Matubayasi, M. Nakahara, J. Chem. Phys. **117**, 3605 (2002); **118**, 2446 (2003)
12. N. Matubayasi, M. Nakahara, J. Chem. Phys. **119**, 9686 (2003)
13. J.P. Hansen, I.R. McDonald, *Theory of Simple Liquids* (Academic Press, London, 1986)
14. K. Hirose, T. Ono, Y. Fujimoto, S. Tsukamoto, *First-Principles Calculations in Real-Space Formalism* (Imperial College Press, London, 2005)
15. J.R. Chelikowsky, N. Troullier, Y. Saad, Phys. Rev. Lett. **72**, 1240 (1994)
16. J.R. Chelikowsky, N. Troullier, K. Wu, Y. Saad, Phys. Rev. B **50**, 11355 (1994)
17. X. Jing, N. Troullier, D. Dean, N. Binggeli, J.R. Chelikowsky, K. Wu, Y. Saad, Phys. Rev. B **50**, 12234 (1994)

18. P. Hohenberg, W. Kohn, Phys. Rev. B **136**, 864 (1964)
19. W. Kohn, L. Sham, Phys. Rev. A **140**, 1133 (1965)
20. H. Takahashi, T. Hori, T. Wakabayashi, T. Nitta, Chem. Lett. **3**, 222 (2000)
21. H. Takahashi, T. Hori, T. Wakabayashi, T. Nitta, J. Phys. Chem. A **105**, 4351 (2001)
22. H. Takahashi, T. Hori, H. Hashimoto, T. Nitta, J. Comp. Chem. **22**, 1252 (2001)
23. H. Takahashi, H. Hashimoto, T. Nitta, J. Chem. Phys. **119**, 7964 (2003)
24. T. Hori, H. Takahashi, T. Nitta, J. Chem. Phys. **119**, 8492 (2003)
25. T. Hori, H. Takahashi, T. Nitta, J. Theor. Comp. Chem. **4**, 867 (2005)
26. H. Takahashi, W. Satou, T. Nitta, J. Chem. Phys. **122**, 044504 (2004)
27. H. Takahashi, Y. Kawashima, T. Nitta, N. Matubayasi, J. Chem. Phys. **123**, 124504 (2005)
28. A.D. Becke, J. Chem. Phys. **98**, 5648 (1993)
29. C. Lee, W. Yang, R.G. Parr, Phys. Rev. B **37**, 785 (1988)
30. C. Peng, H.B. Schlegel, Israel J. Chem. **33**, 449 (1994)
31. Gaussian 03, Revision B.05, M.J. Frisch, G.W. Trucks, H.B. Schlegel, G.E. Scuseria, M.A. Robb, J.R. Cheeseman, J.A. Montgomery, Jr., T. Vreven, K.N. Kudin, J.C. Burant, J.M. Millam, S.S. Iyengar, J. Tomasi, V. Barone, B. Mennucci, M. Cossi, G. Scalmani, N. Rega, G.A. Petersson, H. Nakatsuji, M. Hada, M. Ehara, K. Toyota, R. Fukuda, J. Hasegawa, M. Ishida, T. Nakajima, Y. Honda, O. Kitao, H. Nakai, M. Klene, X. Li, J.E. Knox, H.P. Hratchian, J.B. Cross, C. Adamo, J. Jaramillo, R. Gomperts, R.E. Stratmann, O. Yazyev, A.J. Austin, R. Cammi, C. Pomelli, J.W. Ochterski, P.Y. Ayala, K. Morokuma, G.A. Voth, P. Salvador, J.J. Dannenberg, V.G. Zakrzewski, S. Dapprich, A.D. Daniels, M.C. Strain, O. Farkas, D.K. Malick, A.D. Rabuck, K. Raghavachari, J.B. Foresman, J.V. Ortiz, Q. Cui, A.G. Baboul, S. Clifford, J. Cioslowski, B.B. Stefanov, G. Liu, A. Liashenko, P. Piskorz, I. Komaromi, R.L. Martin, D.J. Fox, T. Keith, M.A. Al-Laham, C.Y. Peng, A. Nanayakkara, M. Challacombe, P.M.W. Gill, B. Johnson, W. Chen, M.W. Wong, C. Gonzalez, J.A. Pople (Gaussian, Pittsburgh PA, 2003)
32. A.D. Becke, Phys. Rev. A **38**, 309 (1988)
33. L. Kleinman, D.M. Bylander, Phys. Rev. Lett. **48**, 1425 (1982)
34. G. Kaminski, E.M. Duffy, T. Matsui, W.L. Jorgensen, J. Phys. Chem. **98**, 13077 (1994)
35. W.L. Jorgensen, J. Chandrasekhar, J.D. Madura, R.W. Impey, M.L. Klein, J. Chem. Phys. **79**, 926 (1983)
36. The reduced temperature for 575 K of TIP4P model is estimated as T_{r}=1.02
37. T.H. Dunning Jr., J. Chem. Phys. **90**, 1007 (1989)
38. H. Takahashi, S. Takei, T. Hori, T. Nitta, J. Mol. Struct.: THOECHEM. **632**, 185 (2003)
39. L. Onsager, J. Am. Chem. Soc. **58**, 1486 (1936)